Biomaterials Science

Radiation-Induced Photodynamic Therapy Using Calcium Tungstate Nanoparticles and 5-Aminolevulinic Acid Prodrug

Journal:	*Biomaterials Science*
Manuscript ID	BM-ART-05-2023-000921.R1
Article Type:	Paper
Date Submitted by the Author:	17-Jul-2023
Complete List of Authors:	Viswanath, Dhushyanth; Purdue University, School of Chemical Engineering Shin, Sung-Ho; Purdue University, School of Chemical Engineering Yoo, Jin; Purdue University, School of Chemical Engineering Torregrosa-Allen, Sandra; Purdue University, Department of Comparative Pathobiology Harper, Haley; Purdue University, Department of Comparative Pathology Cervantes, Heidi; Purdue University, Department of Comparative Pathobiology Elzey, Bennett; Purdue University, Department of Comparative Pathobiology Won, You-Yeon; Purdue University, School of Chemical Engineering

Radiation-Induced Photodynamic Therapy Using Calcium Tungstate Nanoparticles and 5-Aminolevulinic Acid Prodrug

Dhushyanth Viswanath[1], Sung-Ho Shin[1], Jin Yoo[1], Sandra E. Torregrosa-Allen[2,3], Haley A. Harper[2,3], Heidi E. Cervantes[2,3], Bennett D. Elzey[2,3], and You-Yeon Won*[,1,2]

[1]Davidson School of Chemical Engineering, Purdue University, West Lafayette, Indiana 47907, United States, [2]Purdue University Institute for Cancer Research, [3]Department of Comparative Pathobiology, Purdue University, West Lafayette, Indiana 47907, United States.

*Corresponding author

Abstract

Photodynamic therapy (PDT) using 5-aminolevulinic acid (ALA) prodrug is a clinically tried and proven treatment modality for surface level lesions. However, its use for deep-seated tumors has been limited due to the poor penetration depth of visible light needed to activate the photosensitizer protoporphyrin IX (PPIX), which is produced from ALA metabolism. Herein, we report the usage of poly(ethylene glycol–b-lactic acid)(PEG-PLA)-encapsulated calcium tungstate ($CaWO_4$, CWO for short) nanoparticles (PEG-PLA/CWO NPs) as energy transducers for X-ray-activated PDT using ALA. Owing to the spectral overlap between radioluminescence afforded by the CWO core and the absorbance of PPIX, these NPs can serve as an *in situ* visible light activation source during radiotherapy (RT), thereby mitigating the limitation of penetration depth. We demonstrate that this effect is observed across different cell lines with varying radio-sensitivity. Importantly, both PPIX and PEG-PLA/CWO NPs exhibit no significant toxicities at therapeutic doses in the absence of radiation. To assess the efficacy of this approach, we conducted a study using a syngeneic mouse model subcutaneously implanted with inherently radio-resistant 4T1 tumors. The results show a significantly improved prognosis compared to conventional RT, even with as few as 2 fractions of 4-Gy X-rays. Taken together, these results suggest that PEG-PLA/CWO NPs are promising agents for application

of ALA-PDT in deep seated tumors, thereby significantly expanding the utility of an already established treatment strategy.

Introduction

Radiotherapy (RT) is a cornerstone of cancer treatment, with approximately 50% of cancer patients undergoing this therapy[1]. While it is a key component of standard care for various cancers, the prognosis can vary significantly. Some cancers, including breast[2] and head and neck cancers[3, 4], exhibit radio-resistant behavior due to genetic mutations that can arise[5, 6]. As a result, the likelihood of cancer cell death arising from radiation-induced DNA damage is greatly reduced. One strategy to address this issue is to combine radiotherapy with other treatment modalities that operate via alternate mechanisms. Photodynamic therapy (PDT) has emerged as an optimal candidate due to its highly localized effects and ability to kill cancer cells primarily through membrane damage rather than DNA damage[7].

5-Aminolevulinic acid (ALA) and protoporphyrin IX (PPIX) are endogenous compounds formed along the heme synthesis pathway. The conversion of the penultimate intermediate, PPIX, to heme is catalyzed by the enzyme ferrochelatase. Prior studies have suggested that cancer cells express low levels of ferrochelatase activity, thereby preventing this conversion and causing an accumulation of PPIX[8]. This unique property has promoted the usage of ALA as a prodrug for selective PPIX accumulation in cancer cells. Additionally, PPIX serves as both a fluorophore for tumor imaging and a potent photosensitizer for photodynamic therapy. As a photosensitizer, PPIX has been shown to primarily promote type II photodynamic reactions, producing cytotoxic singlet oxygen ($^1O_2$) from molecular oxygen[9]. Since it is highly hydrophobic, it tends to localize in its site of formation, the mitochondria, and to a lesser extent the cytoplasm[10, 11]. As a result, studies investigating the mode of cell death have suggested that apoptosis and necrosis are the most prevalent, attributed to the disruption of the mitochondrial and cell membranes, respectively[12-14].

ALA-PDT is a clinically utilized treatment modality for various cutaneous cancers[15, 16]. Traditionally, an ALA cream or ointment is topically applied to the lesion, followed by an incubation period of 4 – 6 hours in the absence of light. Subsequently, the treated area is exposed to blue or red light to initiate PDT[17]. However, the application of this technique to treat subcutaneous tumors has been limited due to the inadequate penetration depth of visible light photons in tissue[7].

An emerging treatment strategy involves the use of radiotherapy, particularly X-rays, to activate photodynamic therapy using nanoparticles as *in situ* energy transducers[7]. This combination approach addresses the limitations of both treatment modalities; X-rays from external beam radiation can penetrate tissue more effectively than visible light, and the resulting photodynamic effect can effectively eliminate radio-resistant cancer cells. We herein report the development of poly(ethylene glycol-b-lactic acid)(PEG-PLA)-coated calcium tungstate ($CaWO_4$, CWO for short) nanoparticles (PEG-PLA/CWO NPs) as energy transducers for X-ray-activated PDT (RT-PDT) using ALA as illustrated in Figure 1. This work is motivated by our prior study, which showcased the capacity of CWO NPs to activate bilirubin, a less potent photosensitizing compound[3]. We propose that the blue radioluminescence afforded by the CWO core can serve as an *in situ* visible light activation source for the metabolized photosensitizer, PPIX. The excited PPIX can then convert intracellular molecular oxygen into $^1O_2$, resulting in cell death primarily via apoptosis and necrosis as has previously been reported with ALA-PDT[14]. Since PPIX preferentially accumulates in cancer cells, RT-PDT with dose-fractionation can cause highly localized cancer cell death, while sparing nearby healthy tissue. The mechanism and efficacy of the RT-PDT platform was evaluated in cell culture, and in syngeneic subcutaneous mouse models following intratumoral administration. The results suggest that PEG-PLA/CWO NPs are promising tools which can expand the applicability of ALA-PDT from cutaneous tumors to deep-seated tumors.

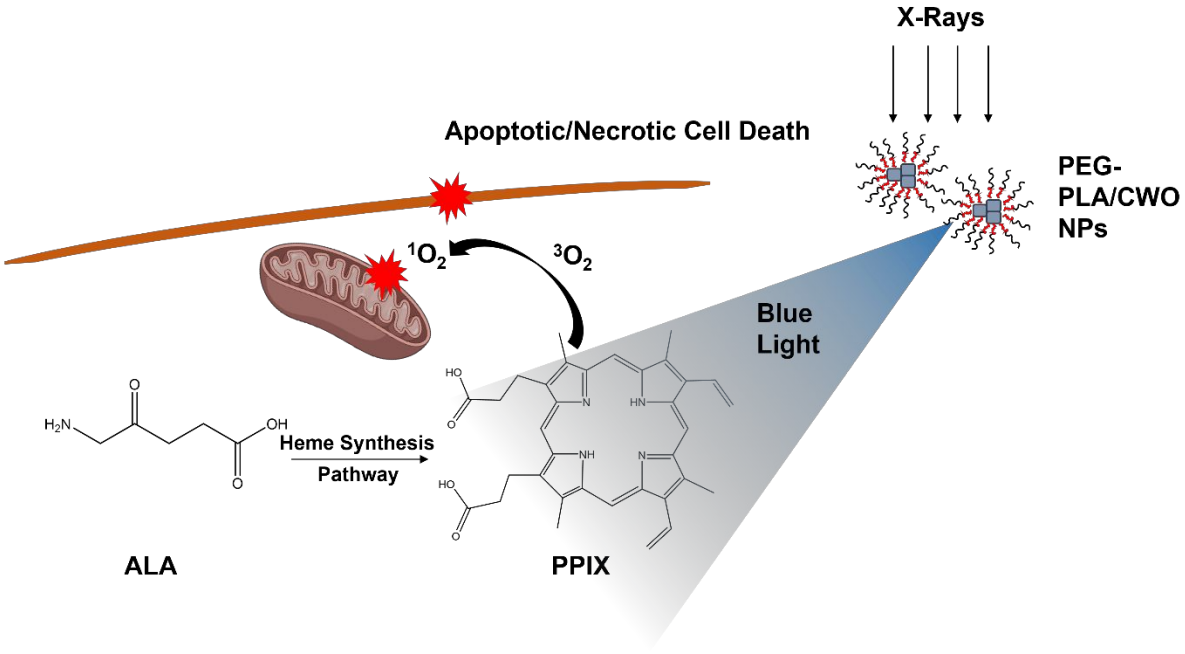

Figure 1. Schematic for the mode of action of PEG-PLA/CWO NPs as energy transducers for RT-PDT.

Materials and Methods

Synthesis and Characterization of PEG-PLA (2k-2k) Block Copolymer

The PEG-PLA block copolymer used in this study was synthesized using ring-opening polymerization of racemic lactide with 1,8-diazabicyclo[5.4.0]undec-7-ene (DBU) as the catalyst and monomethoxy-terminated PEG as the macroinitiator[18]. 4.47 g of methoxy-terminated PEG (M_n = 2,000 Da, Sigma-Aldrich) and 4.47 g of racemic lactide (Sigma-Aldrich) were melted together in a round bottom flask at 60 ºC. A strong vacuum was applied till no bubble formation could be observed (approximately for 30 minutes), after which the flask was purged with nitrogen and cooled to room temperature. 46 mL of anhydrous dichloromethane (DCM, Sigma-Aldrich) was added to dissolve the reactants with the aid of sonication. Once dissolved, the reaction was initiated by adding 6 mL of 0.11 mM DBU (98%, Sigma-Aldrich) dissolved in anhydrous DCM. To obtain the target PLA M_n of ~ 2,000 Da, the reaction was allowed to proceed for 2.5 hours after which it was terminated by adding 30 mg of benzoic acid (Sigma-Aldrich). PEG-PLA was isolated by adding the reaction mixture dropwise to 1 L of mixed hexanes (Fisher) undergoing vigorous mixing. The product was dried under a vacuum oven overnight, crushed into small flakes, and further dried for 24 hours. A small

sample of the final product was dissolved in $CDCl_3$ for ^1H NMR analysis (Bruker AV-III-400-HD) to determine the exact PLA block molecular weight (Figure S1).

Encapsulation of CWO NPs with PEG-PLA

CWO NPs were synthesized and purified as previously described[19]. To encapsulate bare CWO NPs, 100 mg of PEG-PLA was dissolved in 3.9 g of N,N-dimethylformamide (DMF, Fisher). To this, 100 µL of CWO NPs suspended in DMF (10 mg/mL) was added. The mixture was thoroughly dispersed by rapid mixing using an overhead mechanic stirrer (15,000 RPM) with simultaneous sonication in an ultrasonic bath for 10 minutes. 2.1 mL of Milli-Q water was then added and the mixture was further mixed and sonicated for 10 minutes. The final mixture was transferred into a regenerated cellulose dialysis bag (MW cutoff = 30 kDa, Spectrum) and dialyzed for 2 days against 1 L Milli-Q water (replenished after 1, 2, 4 and 24 hours). The resulting encapsulated NPs were isolated from the empty PEG-PLA micelles via centrifugation at 5,000 RPM for 10 minutes, washed twice with Milli-Q water, and re-suspended in Milli-Q water/PBS at the desired concentration.

Nanoparticle Size Characterizations

An estimate for the crystallite size of the pristine CWO NPs could be obtained from the X-ray diffraction pattern using the Scherrer equation as previously described[20]. Samples were prepared by placing a small drop of CWO NPs suspended in chloroform on a glass slide. After solvent evaporation, another drop was added, and this process was repeated till a thin film of NPs was deposited. Measurements were taken on a Rigaku Smartlab operated on PB mode.

Transmission electron microscopy (TEM) was used to visualize the encapsulated NPs and obtain an estimate for primary CWO NP size. Carbon-coated grids (50 mesh) were first pre-treated with glow discharge, after which a drop of sample (CWO or PEG-PLA/CWO NPs in Milli-Q water) was placed on it. The sample was allowed to dry for about a minute, and then replaced with a drop of 2% uranyl acetate. The drop was wicked dry after a minute and the grid was imaged using a Tecnai T20 microscope. For SEM, 20 µL of CWO or PEG-PLA/CWO

NPs (0.1 mg/mL by CWO mass) in Milli-Q water was dried on a Si wafer and coated with Pt under vacuum before imaging on a Nova NanoSEM 450[21].

The hydrodynamic diameters of bare and encapsulated NPs were obtained using dynamic light scattering (DLS, Brookhaven Instruments NanoBrook 90Plus PALS). Measurements were taken at 25 ºC, with a set duration of 3 minutes and averaged across 5 readings.

Quantification of CWO NP Concentration via Flame Atomic Absorption Spectroscopy (AAS)

100 µL of various CWO-containing samples in water were digested in 100 µL of trace metal-free H_2SO_4 and diluted to 5 mL with Milli-Q water. The calcium absorbance was then measured using AAS (PerkinElmer PinAAcle 900F) equipped with a calcium lamp. A series of Ca^{2+} standards (Sigma-Aldrich) were prepared and used to convert from absorbance to molarity. Subsequently, the calcium concentration could be related to calcium tungstate (CWO) concentration by factoring the compound stoichiometry.

Absorbance and Fluorescence Characterizations

Absorbance and fluorescence measurements were taken on a Molecular Devices ID3 spectrophotometer. Protoporphyrin IX-containing samples were prepared by dissolving the compound initially in DMF and subsequently diluting with equal volume of Milli-Q water. The remaining samples were directly suspended/dissolved in the DMF/water mixture.

Cell Culture Experiments

SCC7 cells and HN31 cells (courtesy of Dr. Jeffrey N. Myers at MD Anderson Cancer Center) were used as cellular models for squamous cell carcinoma, whereas 4T1 cells (ATCC) were used as a cellular model for metastatic breast cancer. Cells were cultured using standard aseptic practices in a humidified incubator with 5% CO_2 at 37.0 °C. SCC7 and HN31 cells were cultured in Dulbecco's Modified Eagle Medium (DMEM, Gibco) supplemented with 10% (v/v) fetal bovine serum (FBS, Hyclone), 1% antibiotic/mycotic (Gibco), 1% HEPES (1 M, Gibco), 0.1% 2-mercaptoethanol (55 mM, Gibco) and 0.1% L-glutamine (200 mM, Gibco). 4T1

cells were cultured in RPMI Medium 1640 (Gibco) supplemented with 10% (v/v) fetal bovine serum (FBS, Hyclone), 1% antibiotic/mycotic (Gibco), 1% HEPES (1 M, Gibco), 1% sodium pyruvate (100 mM, Gibco), 0.1% 2-mercaptoethanol (55 mM, Gibco) and 0.1% L-glutamine (200 mM, Gibco).

PPIX Production Assay

Cells were seeded in a 96-well plate at 1.0×10^4 cells/well and incubated overnight. At pre-determined timepoints, the media for the respective groups was discarded and replaced with 200 µL of 1 mM 5-aminolevulenic acid hydrochloride (ALA, Sigma-Aldrich) dissolved in FBS-free media (filtered prior to use with a sterile 0.22-µm nylon syringe filter). After incubation with ALA for varying durations, media from wells were transferred to a separate 96-well plate for analysis of extracellular PPIX concentration. The remaining attached cells were washed with PBS and lysed with 100 µL of 1% sodium dodecyl sulphate (SDS, Sigma-Aldrich) dissolved in PBS. After thorough mixing using a plate shaker, 25 µL of lysed-cell suspension from each well was transferred to a separate 96-well plate for analysis of total protein content via BCA assay (Pierce BCA protein assay kit, Fisher). The fluorescence intensity of the remaining lysed cell solution was measured using a plate reader (Ex/Em = 405/630 nm) and normalized by the total protein content for each well.

MTT Assay

Cells were seeded in a 96-well plate at 0.5×10^4 cells/well and incubated overnight. The next day, media was discarded and replaced with 100 µL of fresh media containing either CWO NPs or PEG-PLA/CWO NPs at varying concentrations. After 24 hours of incubation, 10 µL of 5 mg/mL MTT reagent (Sigma-Aldrich) was added to each well. Following 4 hours of incubation, media was discarded and the attached cells were solubilized in 100 µL of DMSO. The absorbances at 570 nm and 630 nm (for background subtraction) were then measured using a plate reader. Wells without cells, i.e., containing only the respective concentrations of NPs, media, and MTT reagent, were used for blank subtraction at the respective wavelengths.

Singlet Oxygen Detection via Confocal Microscopy

SCC7 cells were seeded in 35 mm poly(D-lysine)-coated glass bottom dishes (MatTek) at 1 × 10^5 cells/dish. Following overnight incubation, media was replaced with 2 mL of FBS-free media containing either ALA (1 mM, filtered prior to use with a sterile 0.22 μm nylon syringe filter), PEG-PLA/CWO NPs (0.2 mg/mL by CWO mass), or a combination of the two. After 4-hour incubation, cells were treated with 40 μL of 0.5 mM singlet oxygen sensor green (SOSG, Fisher) and further incubated for 1 hour. Cells were then irradiated with 8 Gy of X-rays at a dose rate of 2 Gy/minute (320 kV XRAD-320, Precision X-ray). After 20 minutes, cells were washed with PBS and imaged using a Nikon A1Rsi confocal microscope using a 20× dry objective. 405 nm and 488 nm lasers were used to excite PPIX and SOSG, respectively. Since PPIX also absorbs light at 488 nm (albeit to a lesser extent), SOSG emission was detected using a detector channel with a maximum wavelength cutoff of 550 nm to avoid inclusion of PPIX emission in the SOSG channel. Additionally, images across channels were acquired sequentially rather than simultaneously to minimize signal overlap. The laser gain and power settings for both channels were kept constant across all samples.

Clonogenic Cell Survival Assay

Cells were seeded in 6-well plates (N = 3 wells/group) at varying densities based on the cell line and radiation dose as specified in the respective figure captions. After overnight incubation, media was replaced with FBS-free media containing CWO or PEG-PLA/CWO NPs (0.1 mg/mL based on CWO mass), both with and without ALA (1 mM, filtered prior to use with a sterile 0.22 μm nylon syringe filter). A control group of untreated cells grown in media was included in each assay. After incubation with NPs for 4 hours, cells were irradiated at the specified dosage at a dose rate of 2 Gy/minute (320 kV XRAD-320, Precision X-ray). The next day, cells were washed twice with PBS, and then cultured in media for sufficient time to allow at least 6 cell-division cycles (6 – 7 days for SCC7/4T1 cells and 17-18 days for HN31 cells). Media was replaced every 3 days. Cells were then washed with PBS, fixed using a mixture of glacial acetic acid and methanol (1:7 v/v), and stained using a 0.5% crystal violet solution.

Survival fraction was calculated by counting colonies containing more than 50 cells and normalizing by the number of initially plated cells and plating efficiency for each group. It is to be noted that colonies of SCC7 cells specifically were counted with the aid of a microscope at 10× magnification given their tendency to (i) form dense colonies that may not be readily visible to the naked eye and (ii) expand significantly in size due to radiation-induced mitotic catastrophe, thereby appearing as false colonies upon direct visual inspection.

Mode of Cell Death Assay via Confocal Microscopy

4T1 cells were seeded in 35 mm poly(D-lysine)-coated glass bottom dishes (MatTek) at 1 × 10^5 cells/dish. Following overnight incubation, media was replaced with 2 mL of fresh FBS-free media containing the respective treatment (blank media or PEG-PLA/CWO NPs (0.1 mg/mL based on CWO mass) with/without ALA (1 mM, filtered prior to use with a sterile 0.22 μm nylon syringe filter)). Cells were incubated for 4 hours, after which they were irradiated with 8 Gy X-rays at a dose rate of 2 Gy/minute (320 kV XRAD-320, Precision X-ray). Following a 24-hour incubation, cells were washed twice with PBS, and stained with FITC-Annexin V and Ethidium Homodimer-III (Biotium) according to the vendor instruction. Cells were imaged on a Nikon A1Rsi confocal microscope using a 20× dry objective. 488 nm and 514 nm lasers were used to excite FITC-Annexin V and Ethidium Homodimer-III, respectively. Since PPIX also absorbs light at 488 nm (albeit to a lesser extent), FITC-Annexin V emission was detected using a detector channel with a maximum wavelength cutoff of 550 nm to avoid inclusion of PPIX emission in the same channel. Additionally, images across channels were acquired sequentially rather than simultaneously to minimize signal overlap. The laser gain and power for both channels were kept constant across all samples. Brightfield images were processed on Fiji using the following steps: (i) denoising to eliminate background noise, (ii) contrast enhancement by 200% to enhance the cell border intensity, (iii) trainable WEKA segmentation to isolate cells as individual objects, (iv) creating a probability map, (v) converting to a 8-bit image and applying a threshold to create a binary object map, and (vi) filling holes. The final binary mask created above from the brightfield image was applied back to the original

channels to calculate mean fluorescence intensities in all objects (individual cells). A control image of 4T1 cells was processed similarly to obtain mean background fluorescence intensities for FITC and Ethidium Homodimer-III. Cells containing mean fluorescence greater than the above were considered to be positive for the respective channel. Cells negative for both stains were counted as healthy, whereas cells positive for FITC, Ethidium Homodimer-III, or both, were counted as early apoptotic, necrotic, or apoptotic, respectively.

Animal Studies

All procedures used were approved by the Purdue University Institutional Animal Care and Use Committee (PACUC) (Protocol #1112000342) and comply with the guidelines established by the American Association for Accreditation of Laboratory Animal Care (AAALAC). Female BALB/c mice (6 – 8 weeks old, Jackson Laboratory) were housed in a pathogen-free environment under an automatic 12-hour light/dark cycle with standard cages and free access to food and water. Mice were allowed to acclimate to the facility for 1 week prior to starting the respective studies.

In Vivo Pharmacokinetics for Conversion of ALA to PPIX

Female BALB/c mice (6 – 8 weeks) were subcutaneously injected on the right flank with 100 µL of 4T1 cells suspended in sterile PBS at a concentration of 0.5×10^7 cells/mL. Once tumors reached approximately 100 mm^3 (5 days later), mice were dosed with ALA dissolved in PBS via oral gavage (50 mg/mL ALA, 100 µL, filtered prior to use with a sterile 0.22 µm nylon syringe filter). PPIX production was tracked as a function of time via live whole-body fluorescence imaging (Spectral AMI) of mice using an excitation wavelength of 430 nm and an emission filter wavelength of 650 nm.

In Vivo Bioresorbability of CWO NPs

Female BALB/c mice (3-4 months old) were subcutaneously injected on the right flank with either CWO NPs, CWO microparticles (MPs), or PEG-PLA/CWO NPs suspended in PBS (100 µL, 10 mg/mL based on CWO mass). Mice were anesthetized and the right flanks were imaged

using a microCT device (Perkin Elmer Quantum GX) using 18 seconds/scan at an FOV of 36. Mice were imaged immediately, 1 day, 1 week, 1 month after injection, and for every month thereafter. Particle retention was tracked by thresholding out background tissue and integrating the voxel intensity of the locally present particles as a function of time.

Efficacy Study in a 4T1 Syngeneic Model

Female BALB/c mice (6-8 weeks old) were inoculated on right flank with 4T1 cells suspended in PBS (100 µL, 5×10^6 cells/mL). Once tumors reached 75 – 100 mm^3 (day 0), PEG-PLA/CWO NPs suspended in PBS (10 µL, 50 mg/mL based on CWO mass) were administered intratumorally on consecutive days (days 0 and 1). On the day of the second injection (day 1), ALA dissolved in PBS (100 µL, 50 mg/mL, filtered prior to use with a sterile 0.22 µm nylon syringe filter) was administered via oral gavage. Control mice were administered PBS. After a 4-hour incubation period to allow for PPIX formation, tumors were irradiated with 4 Gy of X-rays at a dose rate of 2 Gy/min using a 320 kVp laboratory X-ray irradiator (X-RAD 320, Precision X-ray, North Branford, CT). ALA administration and X-ray irradiation were repeated identically on day 2. Lead shielding was used to ensure precise delivery of X-rays exclusively to the tumor. Digital calipers were used to measure the length (L), width (W) and height (H) of tumors on a daily basis, upon which the volume was calculated as $V = (L \times W \times H) \times \pi/6$. Mice were euthanized if there was a > 20% body weight loss, summed tumor volumes in cm^3 exceeded 10% of the mouse weight in grams, tumors started to ulcerate, or if any impairment in mobility or behavior was observed. Survival analysis for all mice was terminated on day 25 post cell implantation (which corresponds to day 20 post NP injection), after which ulcerations started to randomly appear despite the tumor size[22]. The treatment schedule is summarized in Figure 11. Immediately after the second round of NP injections, 4 mice across different groups injected with NPs were randomly selected and imaged using a microCT device (Perkin Elmer Quantum GX) using 8 seconds/scan at a field of view (FOV) of 72 corresponding to a dose of approximately 5 mGy.

Statistical Analysis

Statistical analysis for all experiments was carried out using two-tailed student's *t* test. Comparisons between mouse survival times from Kaplan-Meier plots were carried out using log-rank analysis on Matlab. Comparisons were considered statistically significant if $p \leq 0.05$ (denoted in figures using *) or highly statistically significant if $p \leq 0.01$ (denoted in figures using **).

Results and Discussion

Synthesis and Characterization of PEG-PLA/CWO NPs

The PEG-PLA block copolymer used was synthesized from DBU-catalyzed ring opening polymerization of lactide, the mechanism for which has been previously discussed in detail[23]. The product was then characterized via ^{1}H NMR to confirm the structure and determine the molecular weight of the PLA block (Figure S1). The molecular weight of the PLA block used for all experiments ranged from 1.8 – 2.0 kDa. CWO NPs with an average crystallite size of ~ 21 nm as determined via XRD (Figure S2) were encapsulated by the block copolymer using a solvent exchange procedure as depicted in Figure 2. The hydrodynamic diameter of the resulting PEG-PLA/CWO NPs was measured using DLS and determined to be 227.70 ± 11.56 nm (Figure 3, N = 4). Additionally, PEG-PLA/CWO NPs were visualized using TEM upon negative staining with 2% uranyl acetate. Representative TEM micrographs are displayed in Figure 4, which clearly show the polymer coating (material with lower electron density) surrounding the CWO NPs. Furthermore, SEM images of uncoated and PEG-PLA-coated CWO NPs were acquired and can be found in Figure S3. Uncoated NPs are observed as aggregates, where individual primary particles are distinguishable. In contrast, the polymer-coated NPs appear as globular structures in which primary particles cannot be readily distinguished. Taken together, these findings validate the successful encapsulation of CWO NPs with PEG-PLA.

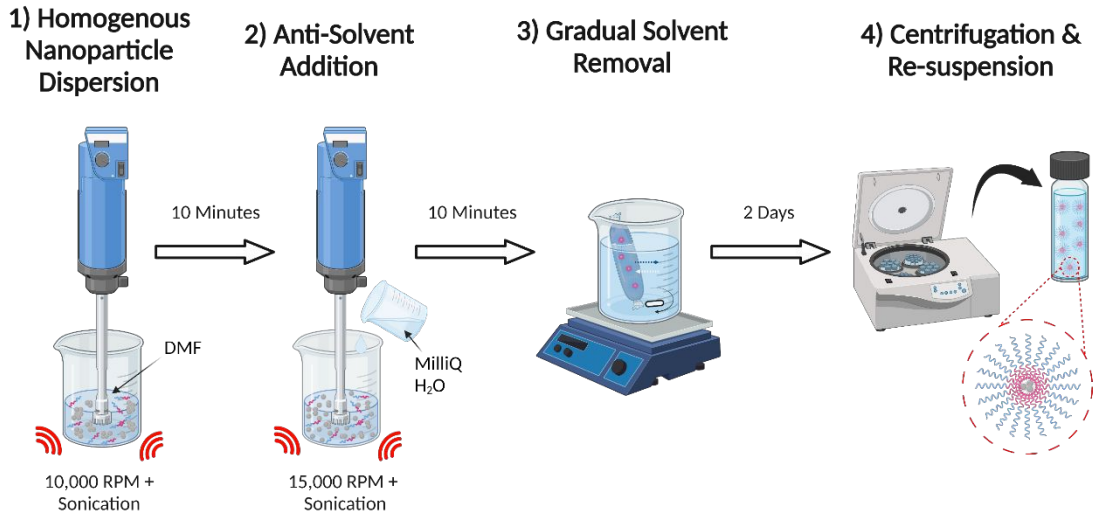

Figure 2. Illustration of the "solvent exchange" procedure used for encapsulation of CWO NPs with PEG-PLA.

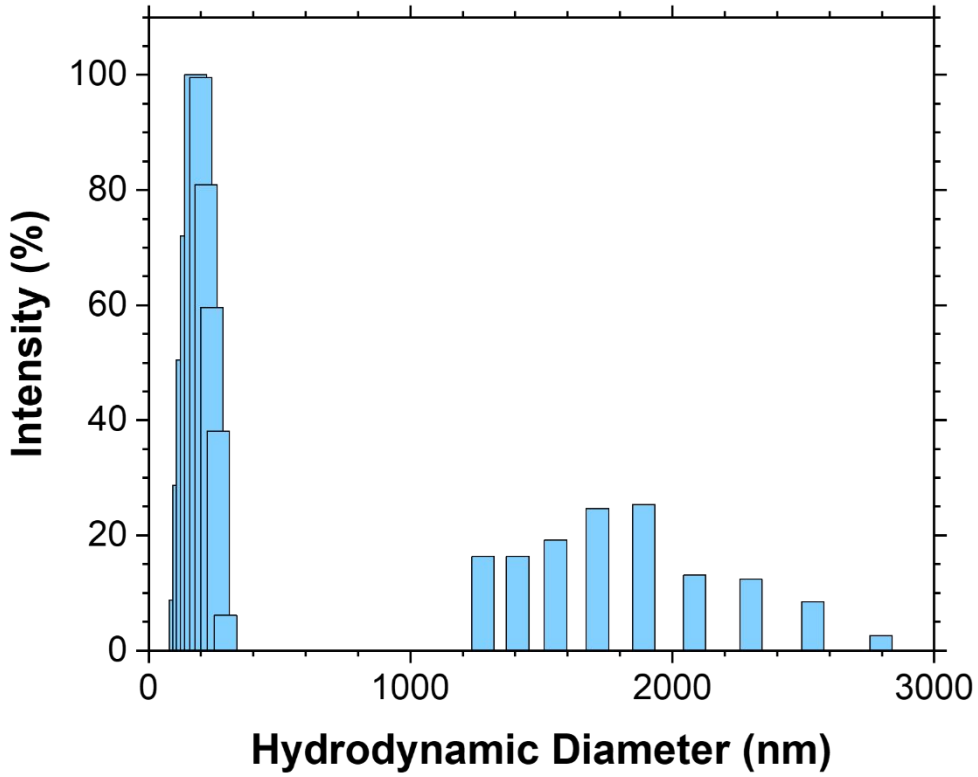

Figure 3. DLS intensity-weighted size histogram for PEG-PLA/CWO NPs (0.2 mg/mL (based on CWO mass) in water). D_h = 227.70 ± 11.56 nm, and PDI = 0.195 ± 0.023 (by cumulant analysis, N = 4).

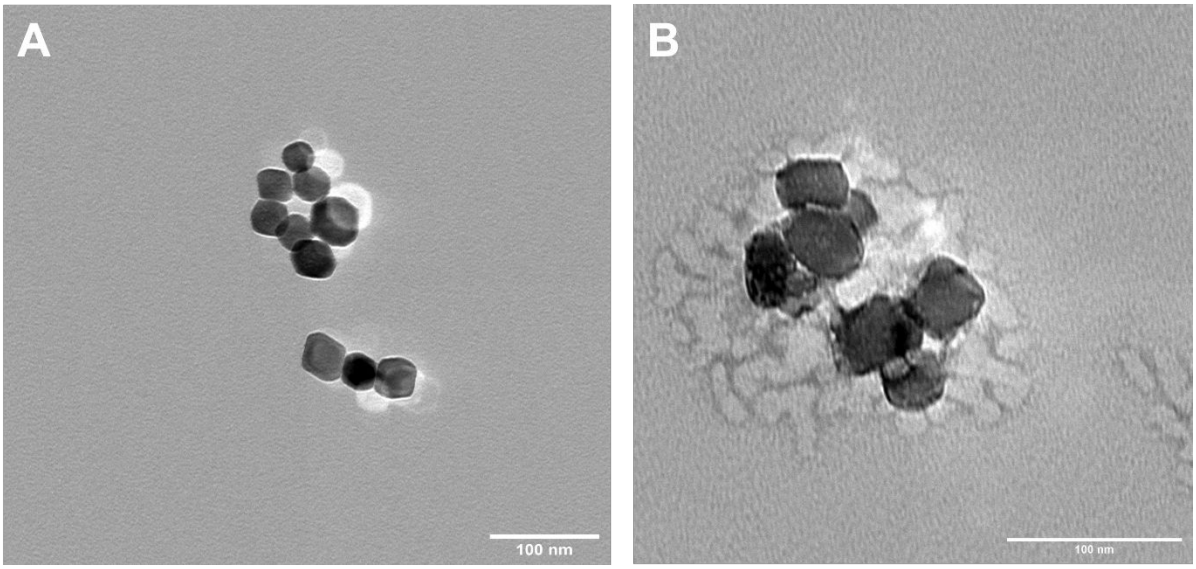

Figure 4. Representative TEM micrographs of (A) uncoated CWO NPs and (B) PEG-PLA/CWO NPs. CWO NPs or PEG-PLA/CWO NPs were dried on carbon-coated copper grids and stained with 2% uranyl acetate. Scale bar = 100 nm.

Absorbance and Emission Characterizations

The absorbance and emission spectra of CWO NPs, ALA, and its metabolized product, PPIX, are shown in Figures 5(A) and 5(B), respectively. The peak absorbance of CWO NPs of around 250 nm was used as the excitation wavelength for emission characterizations. The emission wavelengths of CWO NPs (350 nm ≤ λ ≤ 550 nm; λ_{max} = 420 nm) closely match with the peak absorbance of PPIX (350 nm ≤ λ ≤ 450 nm; λ_{max} = 400 nm), indicating that CWO NPs are a suitable energy-transducer for photoexcitation of PPIX upon X-ray irradiation. When CWO NPs were suspended in a 1 mM PPIX solution, a reduction in CWO fluorescence was observed. Additionally, when PPIX concentration was increased to 10 mM, CWO fluorescence was completely quenched. These results confirm the energy transfer from CWO NPs to PPIX in a concentration-dependent manner, validating the role of CWO NPs as an energy source for activating PPIX.

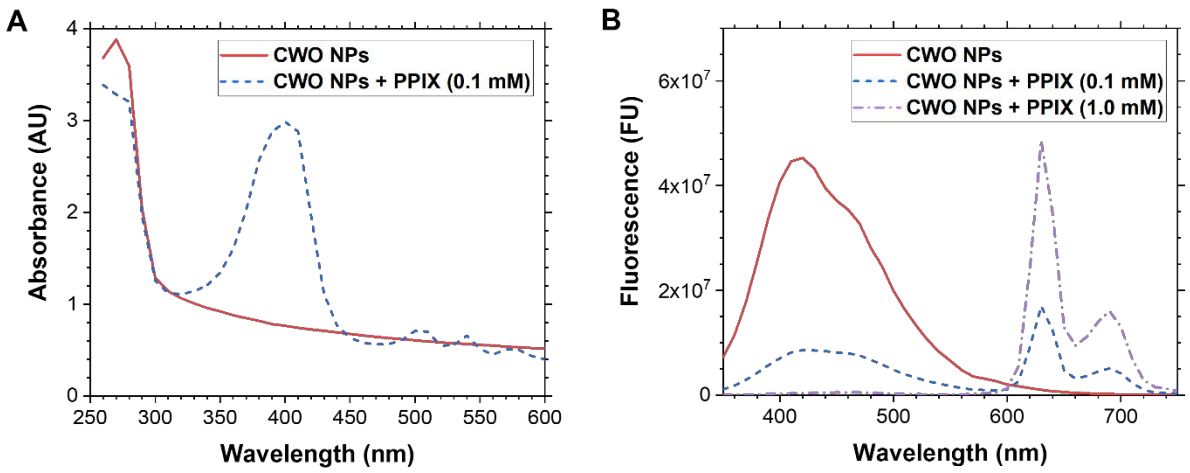

Figure 5. (A) Absorbance and (B) fluorescence spectra of CWO NPs with/without PPIX. NPs were dispersed in a 50:50 by volume mixture of DMF and water. Step size for wavelength scanning = 10 nm. Excitation wavelength for fluorescence measurements = 250 nm.

In Vitro Singlet Oxygen Production and Cytotoxicity

In the clinical setting, it is common to administer ALA pre-treatment to patients 3 – 6 hours prior to illumination to allow sufficient time for the metabolism of ALA to PPIX. To ensure that the cell lines used in this study exhibited noticeable conversion of ALA within this time frame, the fluorescence of the resulting PPIX was monitored over time. As shown in Figure S5, a substantial increase in PPIX fluorescence was observed even after 2 hours of treatment across all tested cell lines. In order to maintain consistency with clinically relevant procedures, an incubation period of 4 hours was selected for all in vitro experiments.

Upon irradiation with X-rays, it is hypothesized that the energy transfer from PEG-PLA/CWO NPs to PPIX can promote the conversion of molecular oxygen to cytotoxic reactive oxygen species such as $^1O_2$. To verify this idea, confocal microscopy was used to detect the fluorescent probe 'Singlet Oxygen Sensor Green' (SOSG) in cells treated with X-rays, PEG-PLA/CWO NPs + X-rays, ALA + X-rays or PEG-PLA/CWO NPs + ALA + X-rays. In the presence of $^1O_2$, SOSG is converted into a compound that fluoresces at 525 nm. Since PPIX is also a fluorophore, the two could be simultaneously detected in cells. However, careful selection of laser and detector settings was necessary to prevent the detection of PPIX in the SOSG channel due to the spectral overlap in their absorbances. As can be observed in Figure

6(A) and Figure S6, the control group of X-rays only and PEG-PLA/CWO NPs + X-rays did not demonstrate any significant fluorescence in either the PPIX or SOSG channels. In cells treated with ALA, distinct red fluorescence was observed in the PPIX channel, indicating the presence of PPIX, and a relatively weaker green fluorescence was observed in the SOSG channel. This result is in agreement with previous studies that suggest the limited capacity of PPIX to directly produce $^1O_2$ when irradiated with X-rays[24]. However, when ALA pre-treatment is combined with PEG-PLA/CWO NPs, the extent of $^1O_2$ production is significantly improved as demonstrated by the increased abundance of the green fluorescence signal. Quantitative analysis of the mean SOSG signal intensity in each cell confirmed this observation (Figure 6(B)). Thus, it can be inferred that PEG-PLA/CWO NPs play a key role in promoting type II photodynamic reaction of PPIX with molecular oxygen upon X-ray irradiation.

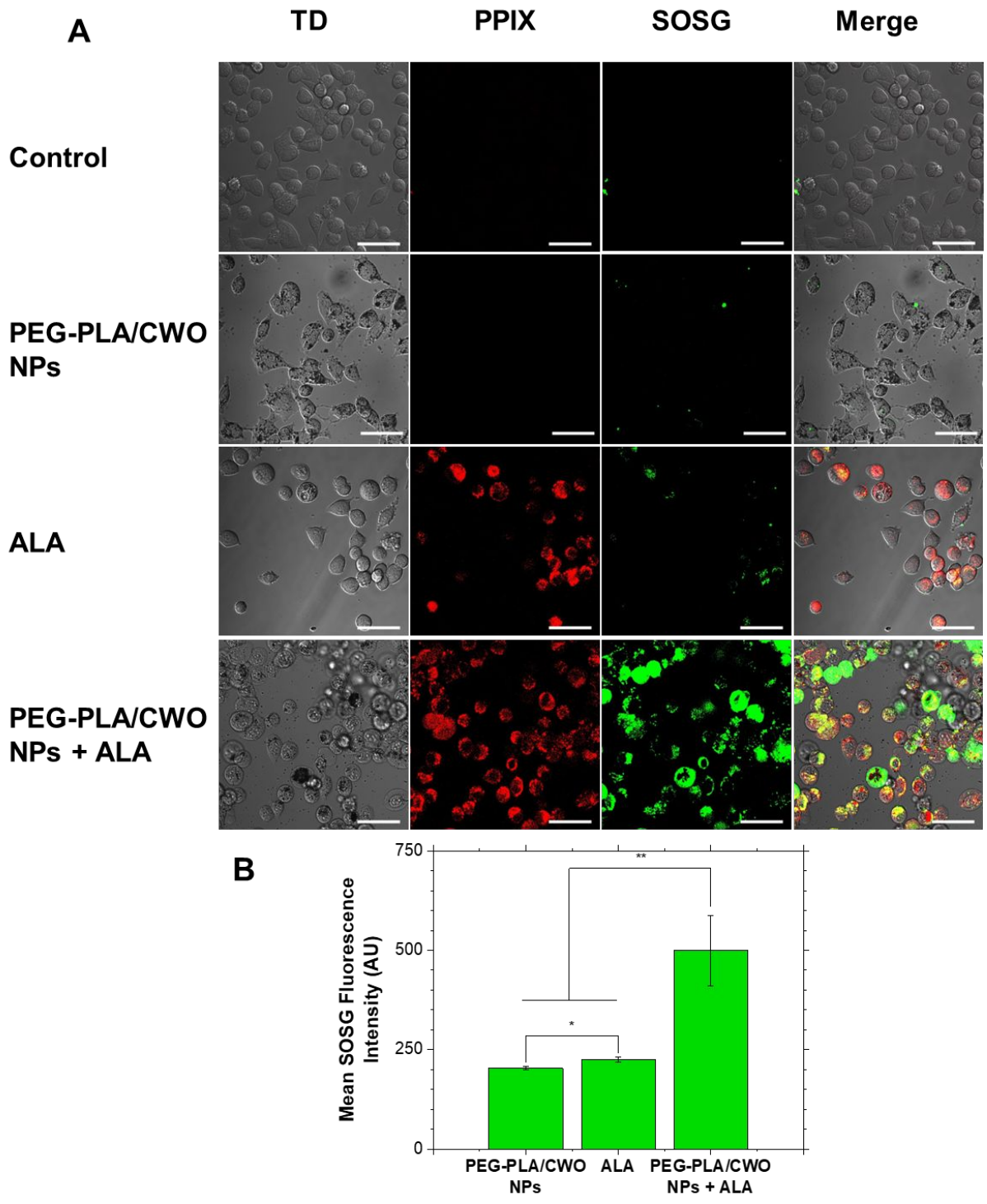

Figure 6. (A) High magnification confocal microscopy images of SCC7 cells treated with PEG-PLA/CWO NPs (0.2 mg/mL based on CWO mass), ALA (1 mM) or a combination of the two. After overnight incubation, all samples were stained with SOSG and irradiated with 8 Gy X-rays. PPIX and SOSG were excited using 405 and 488 nm lasers, respectively. All images were acquired at identical laser settings and displayed with identical lookup table (LUT) values for direct comparison. Scale bar = 50 μm. (B) Mean SOSG fluorescence intensity per cell for SCC7 cells demonstrated in (A). Error bars represent standard errors.

A key advantage in using PEG-PLA/CWO NPs for X-ray-activated PDT (RT-PDT) relies on the absence of any toxicity under “dark” conditions, i.e., in the absence of X-rays. Since X-ray

exposure during RT is localized to the tumor, this minimizes potential side effects on nearby healthy tissues. The dark toxicity of ALA has previously been studied in various cell lines[25-27], from which a concentration of 1 mM was deemed to be suitable for *in vitro* characterizations. The dark toxicity of PEG-PLA/CWO NPs and bare CWO NPs was evaluated at various concentrations via MTT assays. From Figure 7, it can be observed that neither CWO NPs or PEG-PLA/CWO NPs displayed significant loss in cell viability up to concentrations of 1 mg/mL in SCC7 cells and 0.5 mg/mL in 4T1 cells. This finding is in agreement with MTT assays previously conducted in HN31 cells[28]. Consequently, a NP concentration of 0.1 mg/mL was selected for evaluating therapeutic efficacy. These results collectively indicate that PEG-PLA/CWO NPs, in combination with ALA, do not exhibit dark toxicity at the concentrations used for treatment.

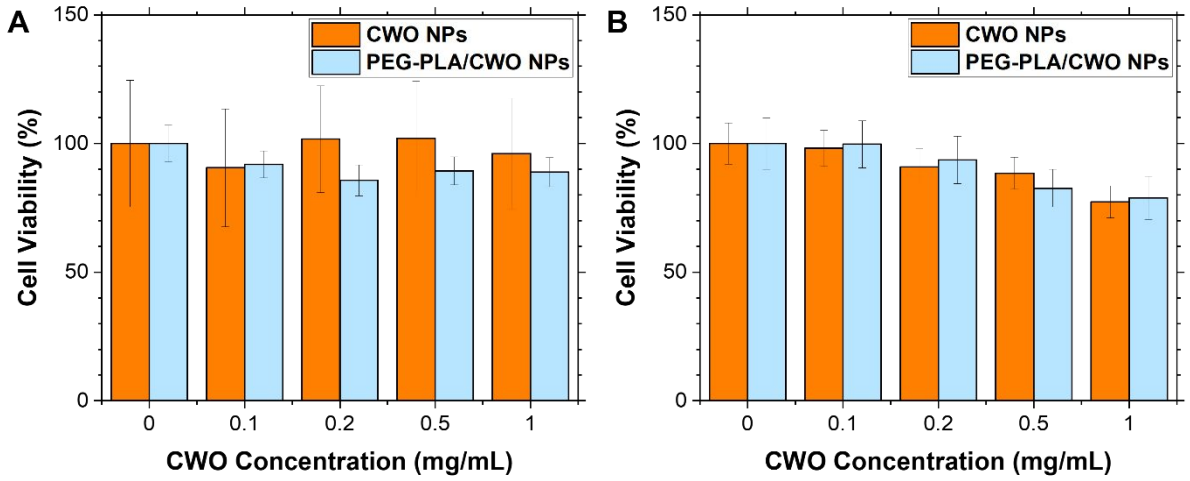

Figure 7. Viability measured by MTT assay of (A) SCC7 and (B) 4T1 cells after 24-hour exposure to varying concentrations of CWO and PEG-PLA/CWO NPs. Formazan absorbance was measured at 570 nm and background subtraction was done at 630 nm. Error bars represent standard deviations (N = 4).

To evaluate the cytotoxicity induced by CWO NPs with ALA pre-treatment upon X-ray irradiation, a series of clonogenic assays were conducted in HN31, SCC7 and 4T1 cells. As can be observed in Figures 8 and S7 – S9, CWO NPs and PEG-PLA/CWO NPs by themselves demonstrated dose-enhancement effects relative to the control, a finding that is in agreement with our previous studies[3, 19, 28]. This enhancement is attributed to the direct cell killing ability of UV-A light[19]. Furthermore, when combined with ALA pre-treatment, the dose-enhancement effects are significantly improved for all cell lines as denoted by the increase in the sensitizer

enhancement ratio (SER) values at 10% cell survival. Moreover, the α/β values also increased in all cell lines for the RT-PDT combination, indicating that the cells were made sensitized to lower doses of radiation. This finding is particularly useful in the context of radiotherapy in clinics, wherein dose fractionation is used to minimize damage to healthy tissue.

When comparing results across different cell lines, it was observed that 4T1 cells, which are more radio-resistant, showed a higher SER for RT-PDT compared to a more radio-sensitive cell line like SCC7. In radio-sensitive cells, X-rays themselves cause a high degree of cell killing even at low doses. As a result, the benefit provided by RT-PDT is less pronounced, although still significant. On the other hand, in radio-resistant cell lines, low-dose X-rays have minimal effects on cell viability. Therefore, the observed dose-enhancement effects of RT-PDT are more substantial in these cell lines. This ability to overcome radio-resistance can be attributed to the ability of RT-PDT to induce cell death through necrosis or P53-independent apoptosis[7]. ALA metabolization to PPIX occurs in the mitochondria, resulting in subcellular localization of PPIX in the mitochondria or cytoplasm[10]. Consequently, $^1O_2$ that is produced during PDT can oxidize the mitochondrial or cell membrane, respectively[11]. The extent of apoptosis and necrosis that follows has been shown to be dependent on cell type and irradiation conditions[29]. A mode of cell death study conducted in 4T1 cells using Annexin V/Ethidium Homodimer staining revealed that PEG-PLA/CWO NPs + X-rays result in elevated levels of apoptosis 24 hours post-irradiation (Figure S10). When combined with ALA pre-treatment, high levels of apoptosis were maintained, and the extent of necrosis increased significantly from approximately 2.5% to around 7.5%. Taken together, these results demonstrate the improved cell-killing potential of the RT-PDT combination therapy and its ability to overcome radio-resistance *in vitro*.

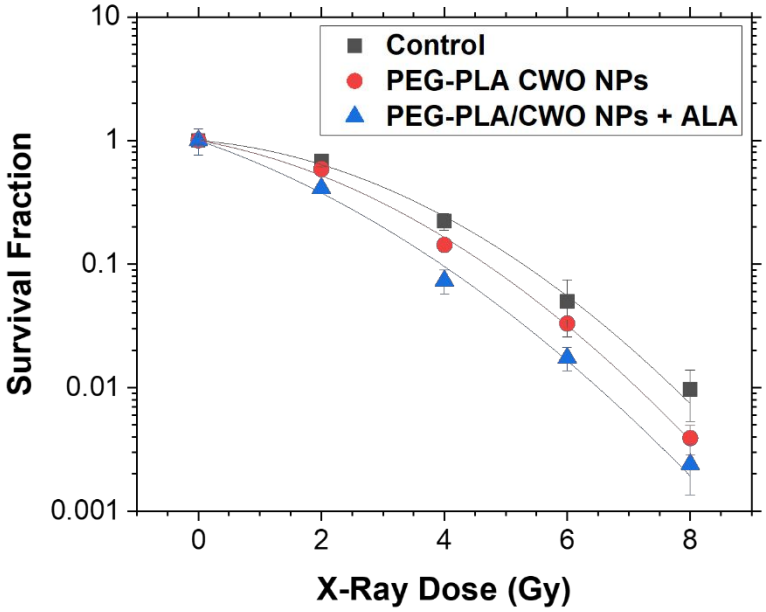

	α	β	α/β	SER
Control	-0.094	-0.065	1.453	1.000
PEG-PLA/CWO NPs	-0.203	-0.062	3.274	1.129
PEG-PLA/CWO NPs + ALA	-0.391	-0.049	8.022	1.338

Figure 8. Clonogenic survival of 4T1 cells post RT-PDT. 4T1 cells were plated in 6-well plates at densities of 0.2 × 10^3, 0.5 × 10^3, 1.0 × 10^3, 2.5 × 10^3 and 5.0 × 10^3 cells/well for 0, 2, 4, 6 and 8 Gy, respectively, incubated with PEG-PLA/CWO NPs (0.1 mg/mL based on CWO mass), ALA (1 mM), or both, for 4 hours, and irradiated with varying doses of X-rays. Surviving colonies were counted after 6 cell division cycles (~ 7 – 8 days). Error bars represent standard deviations (N = 3). The survival curves were fit to the exponential quadratic decay formula, $SF = \exp(\alpha D + \beta D^2)$ where SF = survival fraction, and D = X-ray dose (Gy), using α and β as fitting parameters. The resulting α/β and SER values (calculated at 10% cell survival) are given in the accompanying table.

In Vivo Pharmocokinetics

ALA is considered a favorable prodrug for photodynamic therapy due to its hydrophilicity and its ability to selectively induce the accumulation of protoporphyrin IX (PPIX) in cancer cells[30]. Consequently, systemic administration of ALS proves to be a viable approach for delivering PPIX to tumors, eliminating the necessity for intratumoral injections. Previous studies conducted in mice have shown favorable pharmacokinetics for PPIX formation in tumors following intravenous and oral administration of ALA[31-33]. A small-scale clinical study comparing the two administration routes also suggests that oral delivery is preferable due to

its ease of implementation and comparable pharmacokinetic profiles[31]. As a result, oral administration was selected for the *in vivo* experiments. To verify the formation of PPIX in 4T1 tumors over clinically relevant timescales consistent with our *in vitro* experiments, a pharmacokinetic study was conducted by using live fluorescence imaging to track PPIX fluorescence. From Figures 9 and S11, it is evident that significant PPIX is formed in as little as 1.5 hours post ALA administration. PPIX formation increases significantly as a function of time till the desired incubation period (4 hours). Furthermore, within 24 hours of ALA administration, PPIX fluorescence returned to baseline values, indicating successful clearance within this timeframe. Taken together, these results highly support the oral administration of ALA.

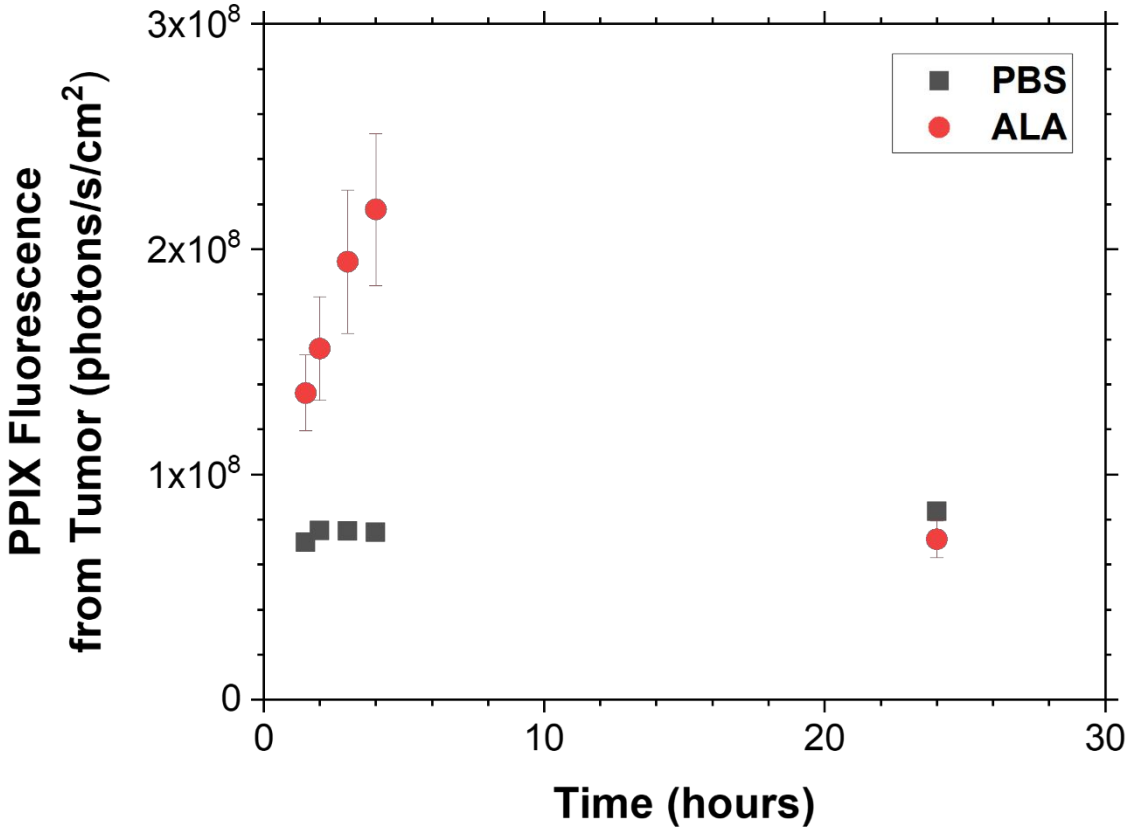

Figure 9. Intratumoral PPIX pharmacodynamics following ALA prodrug administration. 4T1 allografts were established in BALB/c mice as described in the Methods section. Once tumors reached 100 mm^3, ALA (100 µL, 50 mg/mL dissolved in PBS containing 0.5% methyl cellulose) was administered via oral gavage. PPIX formation in tumors was tracked as a function of time using Spectral AMI (λ_{ex} = 430 nm, λ_{em} = 650 nm). Error bars represent standard deviations (N = 3).

Apart from the pharmacokinetics of PPIX formation, an important characteristic is the bioresorbable nature of CWO or PEG-PLA/CWO NPs; i.e., it is essential that NPs can be absorbed into the bloodstream for clearance post-treatment. To test this, CWO NPs, PEG-PLA/CWO NPs or CWO microparticles (MPs, 2 – 3 μm diameter, Sigma-Aldrich) were subcutaneously injected directly into the flanks of mice, at a location identical to a typical tumor implantation. Particle retention at the injection site was tracked as a function of time using CT imaging. From Figure 10, it is evident that PEG-PLA/CWO NPs are cleared rapidly, with 50% clearance occurring within 2 months of administration. CWO NPs demonstrate similar properties, indicating the PEG-PLA coating has minimal effect on bioresorbability. This is reasonable because the timescale for the degradation of the racemic PLA blocks of PEG-PLA block copolymers under physiological conditions is known to be relatively short (50% degradation within 3 – 4 weeks[34]) CWO MPs, on the other hand, demonstrate much slower clearance, taking almost 10 months to achieve 50% resorption, emphasizing the importance of using nanoparticles. It is important to note here that the likely source of particle clearance is uptake by immune cells and/or resorption into the blood (after dissolution of $CaWO_4$ into Ca^{2+} and WO_4^{2-} ions) rather than particle diffusion (because of the transport barrier imposed by the dense subcutaneous tissue (hypodermis) structure); it is known that, for instance, macromolecules/nanoparticles greater than ~ 100 nm are unable to diffuse into lymphatic vessels in the subcutaneous layer[35, 36]. We also note that the CWO residence times within the subcutaneous region are an order of magnitude larger than the predicted CWO dissolution times under continuous flow conditions[19], which suggests that, in the subcutaneous region, the particles are likely surrounded by non-flowing (stagnant) fluids. Furthermore, toxicological evaluations of CWO and PEG-PLA/CWO NPs have been previously conducted through maximum toxicity dose (MTD), hematoxylin and eosin (H&E) staining, and biodistribution studies[28, 37]. H&E analysis of major organ tissue samples from mice injected intravenously with high doses (200 mg CWO/kg body weight) of PEG-PLA/CWO NPs demonstrated the absence of observable toxicities[37]. Biodistribution studies revealed prolonged retention of PEG-PLA/CWO/PTX NPs (PTX = paclitaxel loaded in PLA shell) in tumors, with 60% retention over

1 month after intratumoral injection, while clearance occurred through the liver[28]. Taken together, these studies provide a comprehensive assessment of the particles' safety and demonstrate their non-toxicity at therapeutic doses, which is essential for their potential clinical translation.

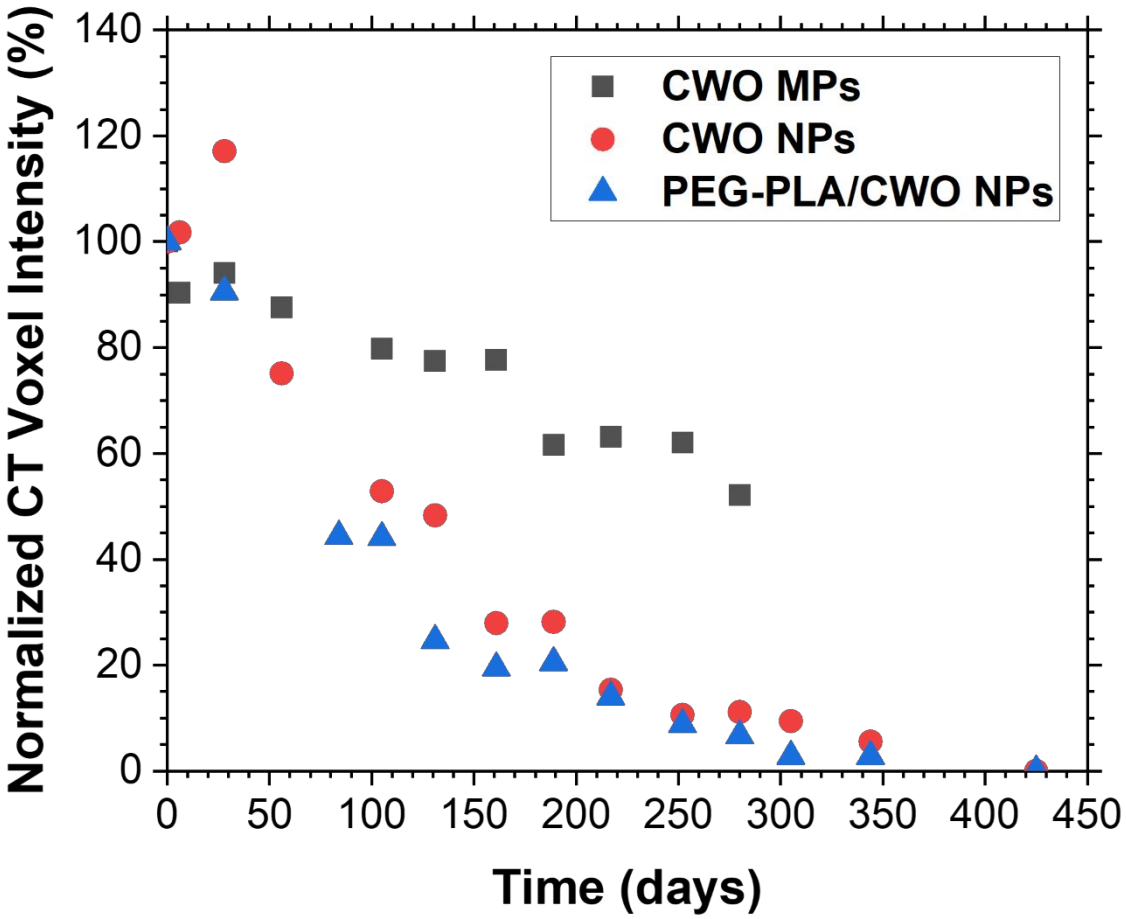

Figure 10. ***In vivo*** **bioresorbability of $CaWO_4$ (CWO). Uncoated CWO nanoparticles (NPs, 21 nm diameter), uncoated CWO microparticles (MPs, 2 – 3 µm diameter) or PEG-PLA/CWO NPs (228 nm hydrodynamic diameter) were subcutaneously injected into the right flanks of BALB/c mice (100 µL, 10 mg/mL based on CWO mass in PBS). Mice were anesthetized under isofluorane, and right flanks imaged using a Perkin Elmer Quantum GX mCT instrument (36 field of view (FOV), 18 seconds per scan). Of note, the mouse injected with CWO MPs died after ~ 10 months post MP injection due to age-related morbidity.**

In Vivo Efficacy

Efficacy studies were conducted in a syngeneic subcutaneous tumor model as illustrated in Figure 11. Mice were administered a combination of either PBS or PEG-PLA/CWO NPs via intratumoral injection and either PBS or ALA via oral gavage. Intratumoral administration of NPs for dose-enhancement in RT presents a clinically feasible strategy for numerous locally

advanced cancers. This strategy typically entails only 1 – 2 injections at the study's commencement, leading to highly localized delivery of NPs directly to the tumor site while minimizing off-target accumulation[38]. After allowing 4 hours for ALA metabolization into PPIX, mice were irradiated with 4 Gy of X-Rays. ALA administration and radiation were repeated the subsequent day (overall radiation dose of 2 $\times$ 4 Gy = 8 Gy). Mouse tumor sizes were tracked as a function of time using digital calipers. From Figure 12, it is evident that none of the unirradiated groups produced any significant therapeutic benefit relative to PBS control, whereas all the irradiated groups did. Among the irradiated groups, only the combination of PEG-PLA/CWO NPs + ALA + X-rays showed a significant improvement compared to the PBS + X-ray group. This improvement was also statistically significant compared to the groups receiving PEG-PLA/CWO NPs + X-rays or ALA + X-rays alone, indicating the importance of each component in achieving RT-PDT. In terms of survival, the study had to be terminated on day 25 post cell implantation (which corresponds to day 20 post NP injection) due to the tendency of subcutaneous 4T1 tumors to form ulcerations, which can lead to erroneous changes in tumor volume[22]. Early indications suggest the potential benefit of RT-PDT (Figure S12 and Table S1), although statistical significance between all groups could not be observed due to study truncation. These findings demonstrate the efficacy of the combined treatment approach and its potential for improving tumor response when compared to individual treatments or controls.

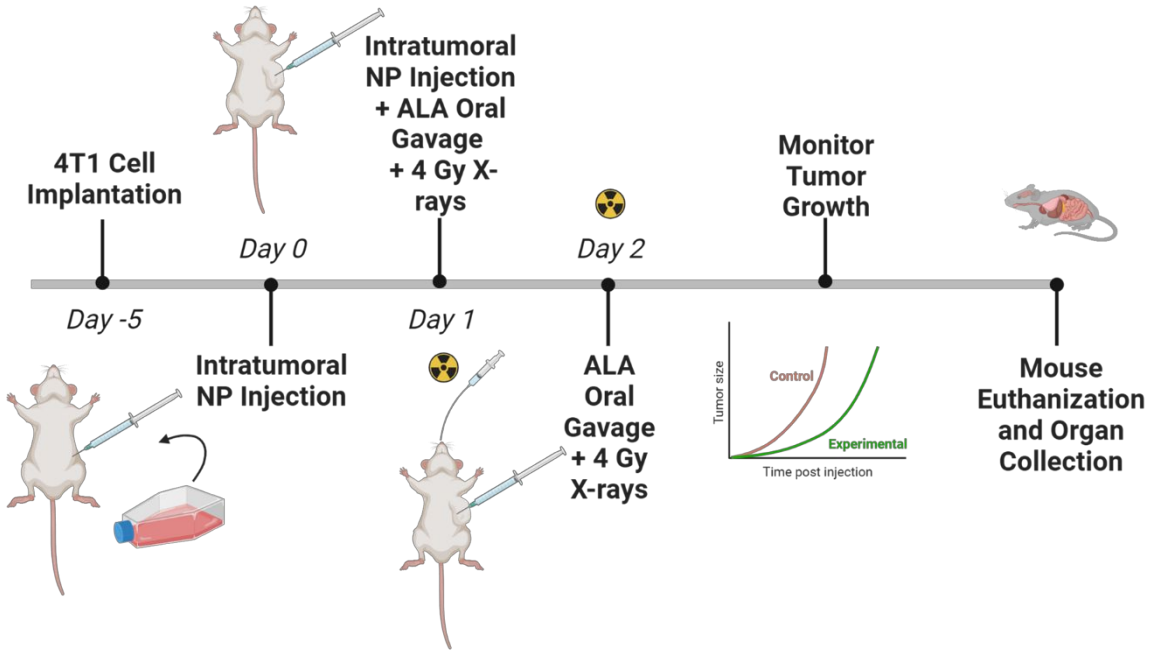

Figure 11. Schematic illustration of the *in vivo* efficacy study protocol.

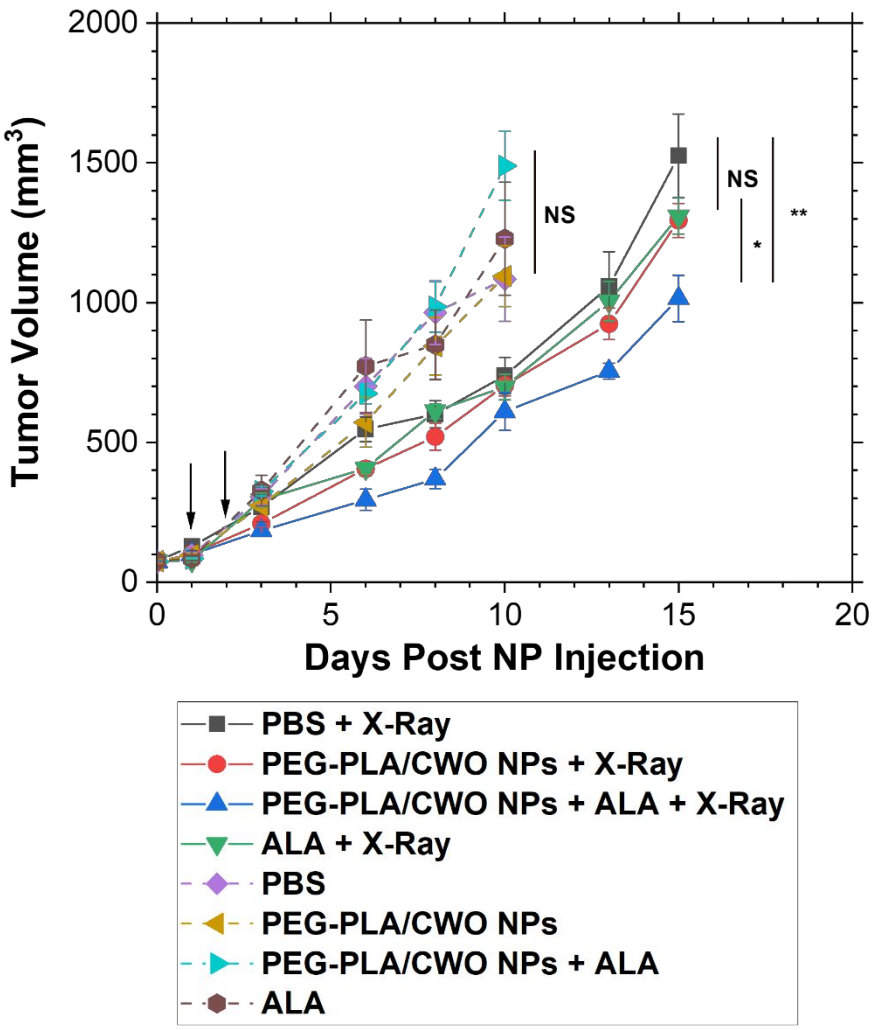

Figure 12. 4T1 allograft tumor growth in BALB/c mice. 4T1 cells (5×10^6 cells/mL in PBS, 100 µL) were subcutaneously implanted into the right flanks of BALB/c mice. Once tumors reached ~ 75 – 100 mm^3, blank PBS or NP suspensions in PBS (50 mg/mL based on CWO mass, 10 µL per injection) were intratumorally injected on Days 0 and 1. An ALA solution in PBS (50 mg/mL, 100 µL per administration) containing 0.5% methyl cellulose was administered via oral gavage on Days 1 and 2. On each of those days, tumors were irradiated with 4 Gy X-rays at 4 hours post ALA administration; radiation times are marked with black arrows. Error bars represent standard errors (N = 5). The one-way ANOVA was used to determine whether a difference exists between groups, and two-tailed t-tests were performed to compute p values between groups across time (i.e., between X-ray-treated groups at Day 15, and between non-X-ray-treated groups at Day 10). NS = difference statistically not significant ($p > 0.05$). * $p < 0.05$. ** $p < 0.01$.

Lastly, CT scans of the tumors were acquired immediately after both NP injections. As can be seen in the representative 3D reconstruction of a typical mouse tumor after NP injections (Figure 13), NPs account for only a small volume of the tumor, corresponding to an average of 1.07 ± 0.23 mm^3 per injection (N = 8 injections analyzed across 4 mice). The corresponding volume fraction of NPs within the tumor after both injections is 2.26 ± 0.49 % (N = 4 mice). Furthermore, assuming each NP injection spreads in 4T1 tumors roughly in the shape of a cylinder with average radius of 0.35 mm and height of 3.00 mm (corresponding volume = 1.15

mm^3 per injection), and that 420 nm photons can penetrate 0.5 mm in tissue[39], the maximum tumor volume illuminated by the injected NPs is 9.1 mm^3 (Figure S13). Further assuming no overlap in photons generated from each injection upon irradiation, the maximum volume of tumor illuminated with blue photons would be 18.2 mm^3 out of 100 mm^3. Due to the limited spreading of nanoparticles, a significant portion of the tumor remains unilluminated, which explains why the differences in tumor volume between the NPs + ALA + X-rays group and other irradiated groups became less pronounced over time. We would like to highlight this as a general limitation for intratumorally administered particles (particularly for those > 100 nm[40]), which is frequently overlooked. In the case of tumors with dense collagen-rich extracellular matrices (ECM) such as the 4T1 tumors in this study[41], overcoming this barrier is crucial for achieving better treatment outcomes. We are currently conducting a separate study to explore surface functionalization approaches for these particles, aiming to enhance their spreading within such tumors. Our hypothesis is that even a slight improvement in particle spreading would significantly enhance tumor illumination, as depicted in Figure S13, leading to improved treatment efficacy.

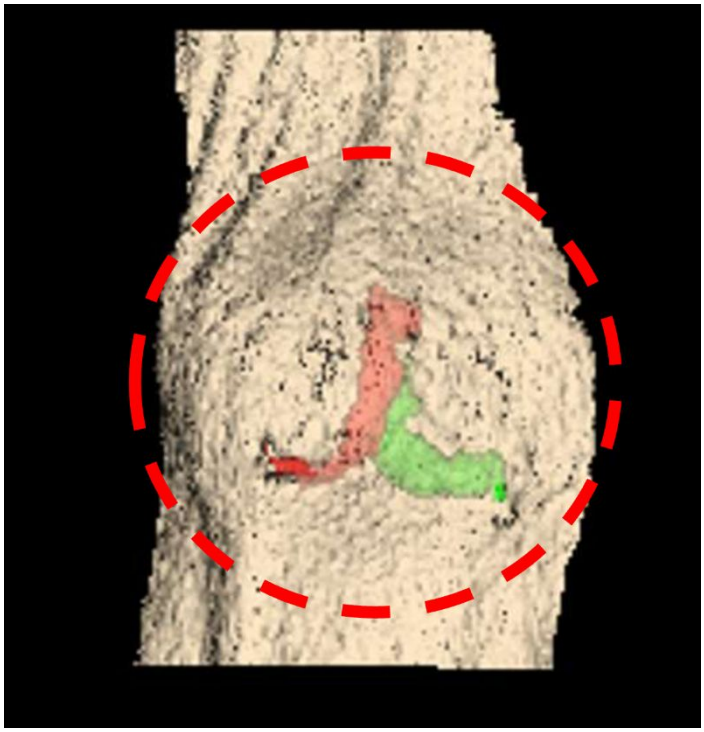

Figure 13. A Representative 3D-reconstructed CT image of intratumorally injected PEG-PLA/CWO NPs. 4T1 cells (5×10^6 cells/mL in PBS, 100 µL) were subcutaneously implanted into the right flanks of BALB/c mice. Once tumors reached ~ 75 – 100 mm^3, blank PBS or NPs suspensions in PBS (50 mg/mL based on CWO mass, 10 µL per injection) were intratumorally injected on Days 0 and 1. Tumors were imaged by CT (72 FOV, 8 seconds per scan) ~ 2 hours after the 2nd NP injection on Day 1; the image was reconstructed at 45 FOV to zoom in on the tumor. The two NP injections were segmented from each other (red and green regions). The dashed red circle shows the visible tumor boundary.

Conclusions

The use of ALA as a prodrug for PDT has been extensively studied for the treatment of surface-level cancers using external beam light sources. This study aims to extend the application of ALA-PDT to deep-seated tumors by utilizing PEG-PLA/CWO NPs as an energy transducer to convert X-ray photons from RT into UV/blue light photons within the tumor. The results indicate that CWO-generated blue photons can activate the photosensitizer, PPIX, triggering a type-II photodynamic reaction that produces cytotoxic $^1O_2$. This mechanism leads to dose-enhancement effects observed in multiple cell lines, including those with high radio-resistance such as 4T1. RT-PDT demonstrates the ability to overcome radio-resistance by inducing membrane damage rather than solely relying on DNA damage caused by conventional RT. Furthermore, both PEG-PLA/CWO NPs and ALA show no toxicity at therapeutic doses in the absence of radiation, which is promising for clinical translation. *In vivo* experiments conducted in mice with subcutaneously implanted 4T1 tumors, known for their radio-resistance and aggressive growth, confirm the findings, showing therapeutic benefits with as few as 2 fractions of 4-Gy X-rays. Based on these results, it is proposed that with further optimization and biological evaluation, PEG-PLA/CWO NPs can serve as a novel tool to enhance the applicability of ALA-PDT from surface-level tumors to deep-seated tumors.

Acknowledgements

Funding for this research was provided by Purdue Office of the Executive Vice President for Research and Partnerships (OEVPRP) (New NIH R01 Program), Purdue University Center for Cancer Research (PCCR, P30CA023168) (Shared Resource Biological Evaluation Project, Phase I Concept Award, and Challenge Research Award), Purdue University Discovery Park (Walther Oncology Physical Sciences & Engineering Research Embedding Program), Lodos Theranostics LLC (Gift Grant), and the Davidson School of Chemical Engineering at Purdue

University. The HN31 cell line was generously provided by Dr. Jeffrey N. Myers at the MD Anderson Cancer Center. YYW is also grateful for funding from NSF (CBET-1803968 and CBET-2211843). DV is also grateful for the Leslie Bottorff Fellowship from Purdue University College of Engineering/Indiana University School of Medicine.

Author Contributions

Dhushyanth Viswanath: Data curation, Formal analysis, Investigation, Methodology, Validation, Visualization, Writing – original draft. **Sung-Ho Shin:** Investigation. **Jin Yoo:** Investigation. **Sandra E. Torregrosa-Allen:** Investigation. **Haley A. Harper:** Investigation. **Heidi E. Cervantes:** Investigation. **Bennett D. Elzey:** Methodology, Resources, Supervision. **You-Yeon Won:** Conceptualization, Funding acquisition, Project administration, Supervision, Writing – review & editing.

Competing Interests

The authors declare no competing interests.

References

1. C. Galeaz, C. Totis and A. Bisio, *Frontiers in oncology*, 2021, **11**, 662840.
2. F. Raeisi, D. Shahbazi-Gahrouei, E. Raeisi and E. Heidarian, *Journal of medical signals and sensors*, 2019, **9**, 68.
3. V. Pizzuti, D. Viswanath, S. E. Torregrosa-Allen, M. P. Currie, B. D. Elzey and Y.-Y. Won, *ACS Applied Bio Materials*, 2020.
4. V. J. Pizzuti, R. Misra, J. Lee, S. E. Torregrosa-Allen, M. P. Currie, S. R. Clark, A. P. Patel, C. R. Schorr, Y. Jones-Hall, M. O. Childress, J. M. Plantenga, N. J. Rancilio, B. D. Elzey and Y. Y. Won, *Acs Biomaterials Science & Engineering*, 2019, **5**, 4776-4789.
5. J. K. A. Jameel, V. S. R. Rao, L. Cawkwell and P. J. Drew, *The Breast*, 2004, **13**, 452-460.
6. F. Perri, R. Pacelli, G. Della Vittoria Scarpati, L. Cella, M. Giuliano, F. Caponigro and S. Pepe, *Head & neck*, 2015, **37**, 763-770.
7. D. Viswanath and Y.-Y. Won, *ACS Biomaterials Science & Engineering*, 2022, **8**, 3644-3658.
8. M. Ishizuka, F. Abe, Y. Sano, K. Takahashi, K. Inoue, M. Nakajima, T. Kohda, N. Komatsu, S.-i. Ogura and T. Tanaka, *International Immunopharmacology*, 2011, **11**, 358-365.
9. M. J. Niedre, A. J. Secord, M. S. Patterson and B. C. Wilson, *Cancer Research*, 2003, **63**, 7986.
10. B. C. Wilson, M. Olivo and G. Singh, *Photochemistry and Photobiology*, 1997, **65**, 166-176.
11. Z. Ji, G. Yang, V. Vasovic, B. Cunderlikova, Z. Suo, J. M. Nesland and Q. Peng, *Journal of Photochemistry and Photobiology B: Biology*, 2006, **84**, 213-220.
12. B. B. Noodt, K. Berg, T. Stokke, Q. Peng and J. M. Nesland, *British Journal of Cancer*, 1996, **74**, 22-29.

13. D. Grebeňová, K. Kuželová, K. Smetana, M. Pluskalová, H. Cajthamlová, I. Marinov, O. Fuchs, J. Souček, P. Jaroĺım and Z. Hrkal, *Journal of Photochemistry and Photobiology B: Biology*, 2003, **69**, 71-85.
14. T. Kriska, W. Korytowski and A. W. Girotti, *Archives of Biochemistry and Biophysics*, 2005, **433**, 435-446.
15. D. E. J. G. J. Dolmans, D. Fukumura and R. K. Jain, *Nature Reviews Cancer*, 2003, **3**, 380-387.
16. E. R. M. De Haas, H. C. De Vijlder, H. Sterenborg, H. A. M. Neumann and D. J. Robinson, *Journal of the European Academy of Dermatology and Venereology*, 2008, **22**, 426-430.
17. Z. Apalla, E. Sotiriou, E. Chovarda, I. Lefaki, D. Devliotou-Panagiotidou and D. Ioannides, *British Journal of Dermatology*, 2010, **162**, 171-175.
18. A. P. Patel, C. R. Schorr, D. Viswanath, K. Sarkar, N. J. Streb, V. J. Pizzuti, R. Misra, J. Lee and Y.-Y. Won, *Industrial & Engineering Chemistry Research*, 2021, **60**, 7081-7096.
19. S. D. Jo, J. Lee, M. K. Joo, V. J. Pizzuti, N. J. Sherck, S. Choi, B. S. Lee, S. H. Yeom, S. Y. Kim, S. H. Kim, I. C. Kwon and Y. Y. Won, *Acs Biomaterials Science & Engineering*, 2018, **4**, 1445-1462.
20. J. Lee, N. J. Rancilio, J. M. Poulson and Y. Y. Won, *ACS Applied Materials and Interfaces*, 2016, DOI: 10.1021/acsami.6b00727.
21. J. Yoo, D. Viswanath and Y.-Y. Won, *ACS Macro Letters*, 2021, **10**, 1510-1516.
22. B. A. Pulaski and S. Ostrand-Rosenberg, *Current Protocols in Immunology*, 2000, **39**, 20.22.21-20.22.16.
23. N. J. Sherck, H. C. Kim and Y.-Y. Won, *Macromolecules*, 2016, **49**, 4699-4713.
24. J. Takahashi, M. Misawa and H. Iwahashi, *Microarrays*, 2015, **4**, 25-40.
25. M. Jalili-Nik, F. Abbasinezhad-moud, S. Sahab-Negah, A. Maghrouni, M. Etezad Razavi, M. Khaleghi Ghadiri, W. Stummer and A. Gorji, *International Journal of Molecular Sciences*, 2021, **22**.
26. V. Herceg, S. Adriouach, K. Janikowska, E. Allémann, N. Lange and A. Babič, *Bioorganic Chemistry*, 2018, **78**, 372-380.
27. M. Hadizadeh and M. Fateh, *Iran J Med Sci*, 2014, **39**, 452-458.
28. R. Misra, K. Sarkar, J. Lee, V. J. Pizzuti, D. S. Lee, M. P. Currie, S. E. Torregrosa-Allen, D. E. Long, G. A. Durm, M. P. Langer, B. D. Elzey and Y. Y. Won, *Journal of Controlled Release*, 2019, **303**, 237-252.
29. L. Wyld, M. W. R. Reed and N. J. Brown, *British Journal of Cancer*, 2001, **84**, 1384-1386.
30. B. Krammer and K. Plaetzer, *Photochemical & Photobiological Sciences*, 2008, **7**, 283-289.
31. C. S. Loh, A. J. MacRobert, J. Bedwell, J. Regula, N. Krasner and S. G. Bown, *British Journal of Cancer*, 1993, **68**, 41-51.
32. M. Miyake, N. Tanaka, S. Hori, S. Ohnishi, H. Takahashi, T. Fujii, T. Owari, K. Ohnishi, K. Iida and Y. Morizawa, *The Prostate*, 2019, **79**, 340-351.
33. C. Perotti, A. Casas, H. Fukuda, P. Sacca and A. Batlle, *British journal of cancer*, 2002, **87**, 790-795.
34. S. Ben-Shabat, N. Kumar and A. J. Domb, *Macromolecular Bioscience*, 2006, **6**, 1019-1025.
35. F. van Dijk, N. Teekamp, L. Beljaars, E. Post, J. Zuidema, R. Steendam, Y. O. Kim, H. W. Frijlink, D. Schuppan, K. Poelstra, W. L. J. Hinrichs and P. Olinga, *Journal of Controlled Release*, 2018, **269**, 258-265.
36. C. J. H. Porter, G. A. Edwards and S. A. Charman, *Advanced Drug Delivery Reviews*, 2001, **50**, 157-171.
37. J. Lee, S. Choi, K. H. Kim, H. G. Heng, S. E. Torregrosa-Allen, B. S. Ramsey, B. D. Elzey and Y.-Y. Won, *Bioconjugate Chemistry*, 2017, **28**, 171-182.
38. N. Scher, S. Bonvalot, C. Le Tourneau, E. Chajon, C. Verry, J. Thariat and V. Calugaru, *Biotechnology Reports*, 2020, **28**, e00548.
39. A. Barbora, O. Bohar, A. A. Sivan, E. Magory, A. Nause and R. Minnes, *PLoS One*, 2021, **16**, e0245350.

40. H. Holback and Y. Yeo, *Pharmaceutical research*, 2011, **28**, 1819-1830.
41. X. Cun, S. Ruan, J. Chen, L. Zhang, J. Li, Q. He and H. Gao, *Acta biomaterialia*, 2016, **31**, 186-196.